Mapping organic coatings on atmospheric particles

Lynn M. Russell, Steven F. Maria, and Satish C. B. Myneni[1,2]
Department of Chemical Engineering, Princeton University, Princeton, New Jersey, USA

Received 6 February 2002; revised 1 April 2002; accepted 5 April 2002; published 22 August 2002.

[1] To date there is no direct evidence of the distribution or characteristics of organic compounds in individual particles because techniques for chemically identifying organic compounds are not sufficiently sensitive to detect molecules or functional groups with masses below 10^{-15} g [*Husar and Shu*, 1975]. Here we present detailed maps of organic groups (aromatic, alkyl, ketonic carbonyl and carboxylic carbonyl groups) and inorganic ions (potassium, carbonate, calcium) in individual dry particles with diameters ranging from 0.2 to 10 μm using a new technique for aerosol characterization by soft X-ray spectromicroscopy at atmospheric pressure. The maps show both the compounds present in individual particles and regions of different compositions within particles. The particle compositions on surfaces are enhanced in shorter chain or more oxygenated groups, providing the first observations of surface active carboxylic acids in organic coatings in atmospheric particles. *INDEX TERMS:* 0305 Atmospheric Composition and Structure: Aerosols and particles (0345, 4801); 0365 Atmospheric Composition and Structure: Troposphere—composition and chemistry

1. Introduction

[2] Experimental evidence and modeling studies show that atmospheric aerosol may play critical roles in changing climate, reducing visibility, and aggravating health [*National Research Council*, 1996]. Their importance is controlled largely by the amount of water taken up in the humid atmosphere and by the subsequent scattering of incident light. The composition and structure of atmospheric particles determine scattering characteristics and chemical reactivity, with the organic fraction of particles being especially important in determining the rate and quantity of water taken up [*Chuang et al.*, 1997; *Cruz and Pandis*, 1998]. Incorporating detailed chemical equilibria for inorganic pollutants such as nitrate species changes the water uptake by particles in the industrialized northern hemisphere, resulting in up to a factor-of-two difference in the predicted aerosol impact [*Adams et al.*, 2001]. Exposed surfaces of individual phases within particles catalyze heterogeneous reactions, serving as oxidizing agents for vapor-phase sulfur, nitrogen and carbon compounds [*Grassian*, 2001]. Identifying the character of these organic compounds in order to predict these chemical and optical properties for individual particles is limited by the detection limits of chemically-specific techniques as well as by our ability to collect and preserve particles in the state in which they exist in the atmosphere [*Gill et al.*, 1983].

[3] Organic characteristics on surface and interior regions change particle scattering, since they describe particles containing two different organic compounds or mixtures with potentially very different optical properties. Particles in the small end of the measured size range (0.2 to 1.0 μm diameter) account for the majority of cloud condensation nuclei number concentrations. Larger particles (0.5 to 2.0 μm diameter) are the most optically efficient, dominating the direct effect of aerosol light scattering. Our measurements characterize particles in these size ranges with detailed composition maps, showing organic coatings of carboxylic acids surrounding particles containing ketones and inorganic ions.

2. Method

[4] Airborne particles were collected for analysis by impaction onto Si_3N_4 windows, providing a transparent substrate for soft X-ray spectromicroscopy to detect absorbances for organic and inorganic groups. While thickness effects preclude conversion of the measured absorbances to moles of bonds, the absorbances themselves and their ratios provide important insights to particle composition and morphology. The NCAR Community Aerosol Inlet [*Blomquist et al.*, 2001] was used to collect particles as large as 5 μm aerodynamic diameter at the C-130 aircraft velocity of 100 m s^{-1}. The air was brought from the inlet to a multi-sample impactor without a pre-cut (PIXE International Corporation, Tallahassee, FL) by aluminum and copper tubing shortened for minimum submicron particle losses. Windows (0.1 μm-thick Si_3N_4) were washed with three drops Milli-Q water and air dried in clean conditions, then mounted on the substrate frame, with the 0.65-mm diameter inlet nozzle adjusted to maximize particle collection at 3 mm from the window for 1 L min^{-1} flow rate while avoiding film breaking.

[5] Spectromicroscopy studies at the C K-, K L-, and Ca L-absorption edges were conducted using a Scanning Transmission X-ray Microscope at the Advanced Light Source (Beamline 7.0.1), Lawrence Berkeley National Laboratory (Berkeley, CA, USA). Aerosol particles collected on silicon nitride windows were placed in a He-filled sample chamber maintained at 1 atm; X-ray transmission of individual aerosol particles was measured as a function of incident photon energies, typically 275–305 eV (C and K), and 340–355 eV (Ca). Point XANES (X-ray Absorption Near Edge Structure) spectra were collected to verify the absorption spectra obtained from the image stacks. The step size of the energies was 0.2 eV close to the absorption edge, and 0.5 eV above and below the absorption edges with dwell times of

[1]Department of Geosciences, Princeton University, Princeton, New Jersey, USA.
[2]Earth Sciences Division, Lawrence Berkely National Laboratory, Berkely, California, USA.

0094-8276/02/2002GL014874

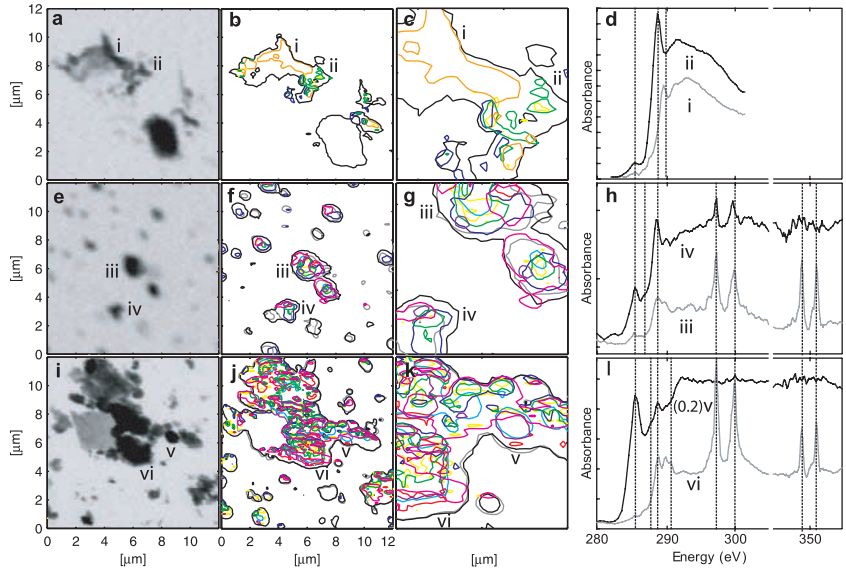

Figure 1. Images, speciated maps of detectable regions, and representative spectra of measured organic and inorganic species for marine boundary layer particles. High-resolution soft X-ray images (a,e,i) show (a) one absorbance image at 300.0 eV (in which Ca^{2+} was not measured) for particles collected in the marine boundary layer near St. Croix at 310 m from 1601 GMT on 19 July 2000 and (e,i) two images at 289.9 eV for particles at 30 m from 1613 GMT on 16 July 2000. Threshold contours (b,f,j) at the detection limits are drawn for the same three samples R(C=C)R′-purple (285.0 ± 0.2eV), R(C=O)R-cyan (286.7 ± 0.2eV), $R(CH_n)R'$-blue (287.7 ± 0.7eV), R(C=O)OH-green (288.7 ± 0.3eV), σ* transition for CNH (in an amide-like group connected to a carbon)-orange (289.5 ± 0.1eV), CO_3^{2-}-yellow (290.4 ± 0.2 eV), K^+-red (294.6, 297.2 ± 0.2 eV), and Ca^{2+}-magenta (347.9, 351.4 ± 0.4 eV). Enlarged maps (c,g,k) and spectra (d,h,l) for representative particles labelled (i–vi) illustrate detailed composition characteristics for each sample.

1–3 ms. A 380 lines mm^{-1} grating and a slit width of 30 by 30 μm were used for imaging and spectral collection.

[6] At the carbon edge, alkyl, ketonic carbonyl, carboxylic carbonyl, and alkene groups were identified. These groups are abbreviated hereafter as $R(CH_n)R'$, R(C=O)R, R(C=O)OH and R(C=C)R′, respectively (with R representing any alkyl chain, R′ representing H or any alkyl chain, and n=0, 1, or 2). The particles contained complex mixtures, so that here the term alkyl represents any C-H bond, as absorbance regions for methyl, methylene, and other alkyl-related groups overlap too much to be distinguished. R(C=O)R measured in these samples overlapped the adjacent $R(CH_n)R'$ absorbance peak forming a shoulder, showing a characteristic absorbance differing from ketones identified to date (probably due to interference from additional groups on the molecule), so that R(C=O)R is used to represent ketone and ketone-like compounds [*Myneni et al.*, 1999; *Warwick et al.*, 1998; *Stöhr*, 1992]. R(C=C)R′ may also indicate aromatic groups, as the exact bond type cannot be distinguished. One additional group is evident in Figures 1b–1d at 289.5, characteristic of a σ* transition for CNH in an amide-like group connected to a carbon [*Stöhr*, 1992].

[7] Images spanning 100 μm^2 were scanned sequentially at up to 220 energy levels to form stacks of images. These image sequences were aligned digitally after processing to account for minor movements during the 4-hr energy scan [*Hitchcock et al.*, 2000]. Each image stack contained up to 20 particles larger than 0.2 μm diameter, each characterized by spectra averaged over four or more 0.008 μm^2 pixels. Spectra were integrated over the characteristic absorption peak energies for each chemical component to produce particle maps, corrected for baseline energy drift and filtered to remove background noise.

3. Aerosol Composition

[8] Flights aboard the NCAR C-130 aircraft near St. Croix during the Passing Efficiency of the Low Turbulence Inlet (PELTI) experiment sampled sea salt particles within the ca. 500 m boundary layer at 30 and 310 m and dust in the free troposphere at 2280 m. Simultaneously collected submicron bulk filters analyzed by X-ray fluorescence (Chester LabNet, Tigard, OR) showed 8 and 16 ng Cl m^{-3} with trace K and Ca in the boundary layer samples. Anthropogenic emission tracers also were present at 310 m on 16 July at 22 ng S m^{-3} and trace V (<1 ng V m^{-3}), although the sample at 30 m on 19 July was consistent with clean marine conditions. The boundary layer samples contained trace amounts of Si, Al, and Fe (22 and 4 ng Si m^{-3}, 7 and 13 ng Al m^{-3}, 9 and 5 ng Fe m^{-3} on 16 and 19 July, respectively), but the free tropospheric sample had significant dust components (150 ng Si m^{-3}, 73 ng Al m^{-3}, 43 ng Fe m^{-3} on 21 July).

[9] Figure 1 shows high-resolution soft X-ray images and contour maps of particle absorbance signatures for R(C=C)R′, R(C=O)R, $R(CH_n)R'$, R(C=O)OH, CO_3^{2-}, K^+, and Ca^{2+} as well as the measured background particle shape for three boundary layer samples. The speciated maps exhibit overlapping small inclusions of several organic groups, sometimes mixed with inorganic species. The prevalence of K^+ and CO_3^{2-} (which make up 1% and 0.4% of dried seawater mass, respectively [*Riley and Chester*, 1971])

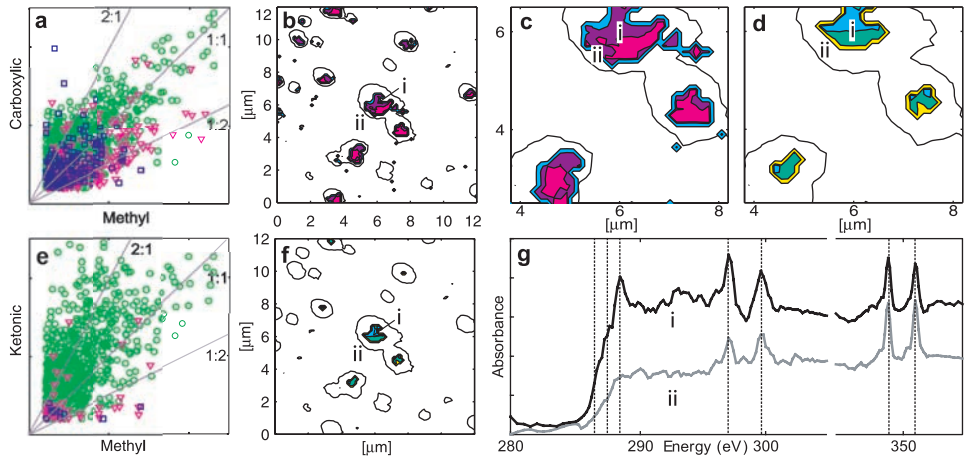

Figure 2. Scatter plots, ratio maps, and representative spectra for R(C=O)OH plotted against $R(CH_n)R'$ and R(C=O)R plotted against $R(CH_n)R'$ for marine boundary layer particle sample in Figures 1e and 1f. Scatter plots (a,e) with ticks representing average spectral intensities of 0.1 and guidelines (gray) compare (a) R(C=O)OH-to-$R(CH_n)R'$ and (e) R(C=O)R-to-$R(CH_n)R'$ for individual pixels in particles from Figures 1a, 1e, and 1i, as blue squares, magenta triangles, and green circles, respectively. Ratio maps show the absorbance ratio of (b) R(C=O)OH-to-$R(CH_n)R'$ for 0.6–2 (pink), 2–60 (purple), and >60 (blue), and (f) R(C=O)R-to-$R(CH_n)R'$ for 0.06–2 (yellow), 2–6 (green), and >6 (cyan). Magnified ratio maps (c) and (d) illustrate coatings on parts of three 1-μm particles from (b) and (f), respectively. Representative spectra (g) are averages of (i) the central region (black spectrum) of the top particle and of (ii) the edge (gray spectrum).

provides good chemical tracers for identifying individual particles derived from sea salt. Particles in Figures 1b, 1f, and 1j contain R(C=O)R, $R(CH_n)R'$, and R(C=O)OH, although Figure 1c illustrates a particle dominated by a σ* transition in CNH. Aromatic groups shown in Figures 1g and 1k indicate the presence of multiple carbon-carbon bonds, either in unsaturated organic compounds or in graphitic carbon. The measured supermicron particles in the sea salt samples are complex and inhomogeneous. Subparticle features on submicron particles cannot be resolved to the same extent as such features are smaller than the detectable area. These nonuniform regions of inorganic and organic material probably represent composites of heterogeneous sources such as soils, combustion products, and secondary organic particles.

[10] Figure 2 shows scatter plots illustrating the correlations at each pixel in the sample range between R(C=O)R and $R(CH_n)R'$ absorbances and between R(C=O)OH and $R(CH_n)R'$ absorbances. Each point in 2(a, e) indicates the approximate intensity at a specific pixel in which both functional groups are found, with the magnitude of the intensity dominated by the mass (and thickness) present and the trend lines indicating a constant ratio or range of ratios. The ratios are proportional to composition ratios not measured spectral intensity. While the scatter in the diagram results both from image noise and from variations in composition, the average trends in the ratios are characteristic of the groups on molecules and the mixtures of molecules present in each region. Deconvoluting molecular from mixture composition requires additional speciation that currently is impossible on the single particle scale, although the higher ratios indicate more oxygenated groups per alkyl group. R(C=O)OH-to-$R(CH_n)R'$ data lie above an absorbance ratio of 0.5, meaning that on average these compounds were either highly oxygenated or shorter carbon chain molecules (relative to molecules or mixtures found below the ratio). A similar lower limit for the R(C=O)R-to-$R(CH_n)R'$ ratio is also evident at 0.5. Short carbon chain molecules are consistent with existing studies of organic compounds associated with sea salt [*Kawamura and Gagosian*, 1990]. The alternative conclusion that longer chain molecules (if present) must be highly oxygenated is also consistent with the large fractions of dissolved organic compounds (DOC) that are present in seawater [*Ming and Russell*, 2001].

[11] Representative sections of the marine particle were mapped in Figures 2b, 2c, 2d, and 2f with contour ratios of R(C=O)R and R(C=O)OH referenced to $R(CH_n)R'$. The higher ratios of carbonyl groups to alkyl groups are found on the surface for carboxylic groups but in the interior for ketonic groups. While this X-ray spectroscopic analysis (dry in He) does not show particle structure in humid conditions, this atmospheric pressure measurement will retain some semi-volatile compounds that may evaporate during electron microscopy in vacuum, including species forming organic films (such as oxalic acid). Since the spectra are taken in dry conditions, those particles that were originally dissolved in liquid water may have coated an aqueous droplet at the air/water interface or a non-aqueous phase liquid at the organic/water interface.

[12] The mapped ratios shown in Figure 3 provide clear boundaries between ketone-like compounds and carboxylic acids in atmospheric particles, both of which contain polar double-bonded oxygen (carbonyl) located on an internal carbon (ketonic) or a terminal carbon (carboxylic). The carboxylic acids are more polar and more surface active as they contain both a double-bonded oxygen and a single-bonded oxygen (alcohol). The surface behavior is characterized by the lower surface tensions of short-chain surfactant liquids at 298 K [*Reid et al.*, 1987]. The segregation of these more strongly polar carboxylic acids to the particle surface may be both cause and effect:

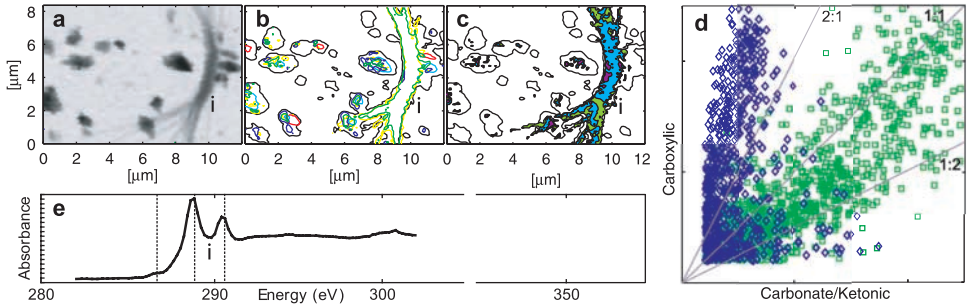

Figure 3. Image, speciated and ratio maps, and scatter plot for dust sample at 2280 m from 1609 GMT on 21 July 2000. High-resolution soft X-ray image (a) and speciated map (b) summarize spectral stack with contours as in Figure 1. Ratio map (c) shows the variation in the absorbance ratio of R(C=O)OH-to-CO_3^{2-} for 0.4–0.6 (green), 0.6–1 (blue), and >1 (magenta). Scatter plot (d) shows correlations for R(C=O)OH-to-CO_3^{2-} (green squares) and R(C=O)OH-to-R(C=O)R (blue diamonds), as in Figures 2a and 2e. The spectrum (e) shown for the particle region labelled (i) illustrates the absorbance peaks for R(C=O)R, R(C=O)OH, and CO_3^{2-}.

R(C=O)OH is frequently found in surfactants making them likely to coat the surface, and terminal carbons may be sterically favored for oxidation by surface reactions. In contrast, the ketonic compounds are more likely to be soluble in aqueous solutions with inorganic ions.

[13] The dust sample in Figure 3 shows only a few large particles, with the largest approximately 3 μm by 10 μm containing Ca^{2+}, CO_3^{2-}, R(C=O)OH, and R(C=O)R. This particle has a shell-like structure that could be $CaCO_3$ in aragonite form embedded in organic membranes or alternatively a calcium-organic precipitate. The composition of this particle is unique in its strong correlation between R(C=O)OH and CO_3^{2-} in individual pixels, with the maps and scatter plots of these relative abundances as well as of R(C=O)OH relative to R(C=O)R shown in Figure 3d.

4. Discussion

[14] These results show that particles collected in marine conditions in the Caribbean contained complex mixtures of R(C=O)R, $R(CH_n)R'$, and R(C=O)OH, revealing heterogeneous phases in maps of the dried particles. Organic coatings covered many of the organic clumps found in 0.3–1.0 μm dry diameter particles with enhanced concentrations of R(C=O)OH. Organic compounds were not limited to surface coatings, although the particle interiors were enhanced in R(C=O)R rather than R(C=O)OH.

[15] This varied organic composition within individual particles illustrates a diverse character of the organic fraction that is inconsistent with known collection related artifacts. This result is consistent with shorter or more oxygenated carboxylic carbonyl compounds that are active at the surface as well as with oxidation of external organic compounds by heterogeneous reactions. Coatings on organic phases within particles provide direct evidence for surface active compounds that may serve to coat aqueous particles in humid conditions. The detailed structure obtained by this method will have different optical properties, hygroscopic behavior, and surface chemistry than the simpler compositions assumed by global and regional models to date. Our measurements provide evidence of coated structures within dry atmospheric particles, which may affect condensation and evaporation of semivolatile vapors including water.

[16] **Acknowledgments.** This study was supported by the National Science Foundation grant ATM97-32949. The authors are grateful for advice and facilities provided by J. R. Anderson, B. J. Huebert, K. K. Laursen and NCAR. The Advanced Light Source of Lawrence Berkeley National Laboratory provided synchrotron time and technical support.

References

Adams, P. J., et al., General circulation model assessment of direct radiative forcing by the sulfate-nitrate-ammonium-water inorganic aerosol system, *J. Geophys. Res.*, *106*, 1097–1111, 2001.

Blomquist, B. W., et al., An evaluation of the community aerosol inlet for the NCAR C-130 research aircraft, *J. Atmos. Oceanic Tech.*, *18*, 1387–1397, 2001.

Chuang, P. Y., R. J. Charlson, and J. H. Seinfeld, Kinetic limitations on droplet formation in clouds, *Nature*, *390*, 594–596, 1997.

Cruz, C. N., and S. N. Pandis, The effect of organic coatings on the cloud condensation nuclei activation of inorganic atmospheric aerosol, *J. Geophys. Res.*, *103*, 13,111–13,123, 1998.

Cruz, C. N., and S. N. Pandis, Deliquescence and hygroscopic growth of mixed inorganic-organic atmospheric aerosol, *Environ. Sci. Tech.*, *34*, 4313–4319, 2000.

Gill, P. S., T. E. Graedel, and C. J. Weschler, Organic films on atmospheric aerosol particles, fog droplets, cloud droplets, raindrops, and snowflakes, *Rev. Geophys.*, *21*, 903–920, 1983.

Grassian, V. H., Heterogeneous uptake and reaction of nitrogen oxides and volatile organic compounds on the surface of atmospheric particles including oxides, carbonates, soot and mineral dust: Implications for the chemical balance of the troposphere, *Int. Rev. Phys. Chem.*, *20*, 467–548, 2001.

Hitchcock, A., et al., aXis2000 Software Version 2.0c, http://unicorn.mcmaster.ca/aXis2000.html, 4 December 2000.

Husar, R. B., and W. R. Shu, Thermal analysis of the Los Angeles smog aerosol, *J. Appl. Meteorol.*, *14*, 1558–1565, 1975.

Kawamura, K., and R. B. Gagosian, Midchain ketocarboxylic acids in the remote marine atmosphere: Distribution patterns and possible formation mechanisms, *J. Atmos. Chem.*, *11*, 107–122, 1990.

Ming, Y., and L. M. Russell, Predicted hygroscopic growth of sea salt aerosol, *J. Geophys. Res.*, *106*, 28,259–28,274, 2001.

Myneni, S. C. B., T. A. Warwick, G. A. Martinez, and G. Meigs, C-functional group chemistry of humic substances and their spatial variation in soils, *Advanced Light Source Activity Report*, 337–340, 1999.

National Research Council, *A Plan for a Research Program on Aerosol Radiative Forcing and Climate Change*, National Academic Press, Washington, D.C., 1996.

Reid, R. C., J. M. Prausnitz, and B. E. Poling, *The Properties of Gases and Liquids*, McGraw-Hill, New York, 1987.

Riley, J. P., and R. Chester, *Introduction to Marine Chemistry*, Academic, San Diego, Calif., 1971.

Stöhr, J., *NEXAFS Spectroscopy*, Springer-Verlag, Berlin, 1992.

Warwick, T., et al., A scanning transmission x-ray microscope for materials science spectromicroscopy at the advanced light source, *Rev. Sci. Instrum.*, *69*, 2964–2973, 1998.

L. M. Russell, Department of Chemical Engineering, Princeton University, Princeton, NJ 08544, USA. (lrussell@princeton.edu)